

## Accepted Manuscript

Title: Algorithm-aided Performance Enhancement of a Trace Explosives Sensor

Authors: Burhan F. Necioğlu, Wansheng Su, Jefferson Rhodes, Sarah O'Donnell, Mark Taczak, Samar K. Guharay



PII: S0925-4005(17)32381-X  
DOI: <https://doi.org/10.1016/j.snb.2017.12.055>  
Reference: SNB 23743

To appear in: *Sensors and Actuators B*

Received date: 17-7-2017  
Revised date: 14-11-2017  
Accepted date: 11-12-2017

Please cite this article as: Burhan F.Necioğlu, Wansheng Su, Jefferson Rhodes, Sarah O'Donnell, Mark Taczak, Samar K.Guharay, Algorithm-aided Performance Enhancement of a Trace Explosives Sensor, Sensors and Actuators B: Chemical <https://doi.org/10.1016/j.snb.2017.12.055>

This is a PDF file of an unedited manuscript that has been accepted for publication. As a service to our customers we are providing this early version of the manuscript. The manuscript will undergo copyediting, typesetting, and review of the resulting proof before it is published in its final form. Please note that during the production process errors may be discovered which could affect the content, and all legal disclaimers that apply to the journal pertain.

## Algorithm-aided Performance Enhancement of a Trace Explosives Sensor

Burhan F. Necioğlu, Wansheng Su, Jefferson Rhodes, Sarah O'Donnell, Mark Taczak,  
Samar K. Guharay\*

The MITRE Corporation, McLean, VA 22012, USA

\*Correspondence: Samar K. Guharay, [sguharay@mitre.org](mailto:sguharay@mitre.org)

### Highlights:

- Waveforms comprising sensor's response to injected materials are exploited through a systematic study.
- A machine-learning based approach is applied to examine the sensor data.
- Results and analysis demonstrate much improved sensor performance by implementing an appropriate signal processing algorithm.
- Exploitation of sensor data by advanced signal processing can be effective and efficient for augmenting sensor performance without changing the hardware.

Approved for Public Release; Distribution Unlimited. Case Number 15-2993

©2017 The MITRE Corporation. ALL RIGHTS RESERVED

**Abstract**

This article describes the exploitation of data obtained from a mature trace explosives detection device with the goal of enhancing the device's performance via signal processing and no hardware modification. This is achieved by implementing a machine-learning algorithm based on nearest-neighbor binary classification. This study aims to determine the parameters of the algorithm defining key feature vectors for both explosive and non-explosive materials via systematic experimentation and measurements. Receiver operating characteristic (ROC) curves are estimated showing the trade-off between detection / false alarm rates, and the results demonstrate the merit of this approach for advancing the performance of this technology. Furthermore, the algorithm is shown to enable not just improved detection, but also a capability for target or materials identification.

**Keywords:** sensor; explosives detection; identification; signal processing; performance improvement

**1 Introduction**

Sensing technologies have broad relevance to many application domains including security screening, environment monitoring, contamination analysis, and disease detection. However, sensors are usually effective only for the specific targets and conditions for which they are designed, and a major challenge is maintaining effectiveness in scenarios with dynamically changing characteristics of targets and operational environments. One such scenario pertains to the detection of explosives in security screening, a scenario which can be further complicated by the fact that the target materials (traces/residues of

explosives) can be obscured by clutter (i.e., the presence of other materials that overwhelm the desired signal or that cause similar, false responses), especially in uncontrolled environments. This article discusses research toward transforming an existing explosive sensing technology and significantly improving its performance solely through changes to the signal processing algorithms used to detect target materials. This work develops the structure of the algorithm and illustrates its merit through systematic experimental measurements and analysis.

Developing a new sensing technology to detect a target includes several key steps: identification of an appropriate phenomenology for detecting the target, design and implementation of reliable and reproducible configurations of a sensing device that generates data from the phenomenology-derived response, and exploitation (by signal processing) of the data to indicate a detection. For explosives detection, a vast literature exists on the fundamentals of sensing phenomenology [1-2], technology architectures [3-5], signal processing [6-8], and sensor testing and evaluation [9-11]. Given an effective phenomenology and its implementation in a sensing device, it is important to ask: (a) if the data generated by the sensor have been fully exploited, and, if not, (b) if the performance of the device can be improved solely through further processing of unexploited data instead of engineering and/or acquiring a new device. These questions motivate the present work to improve the performance of a trace explosive sensing device by developing and implementing new signal processing algorithms – an approach that establishes an effective and efficient path for improving existing technology.

A large number of mature technologies exists for trace explosives and chemicals detection. This investigation focuses on a mature technology based on the principles of amplifying fluorescent polymers (AFP) – a technology used most commonly in the Fido series of sensors from FLIR [12]. A good number of articles has been published reporting the performance of this device [13-16]. The mechanism of fluorescence quenching by conjugate polymers and its role in explosives detection have been discussed [17-24], and strong research activities in this area persists.

The present work is based on the Fido XT platform, an older AFP-based device that has since undergone additional generations of development and refinement. The output interface of the Fido XT device permits the acquisition of both raw sensor response as well as the data processed by the native algorithm of the device. We developed a machine-learning algorithm based on a non-parametric nearest-neighbor binary classification (detection) scheme to locally process both sets of output data and derive enhanced detection results compared to the unmodified device. In addition to improved detection capability, the algorithm also shows potential for enabling more fine-grained classification and identification of specific explosive and non-explosive materials.

Section 2 of this report describes the experimental methods used, including the data collection approach. Section 3 describes the signal processing and algorithm development for detection and identification. Analysis of the experimental results and discussions are given in Section 4, with Section 5 providing a summary of the work and its implications.

## **2 Experimental Method**

Figure 1 shows the schematics of the AFP-based Fido XT sensing device and experimental arrangement. Analyte standards with several different concentrations (10  $\mu\text{g/mL}$ , 100  $\mu\text{g/mL}$ , and 1  $\text{mg/mL}$ ) were used, and the sensor output exhibited a response linearly proportional to sample concentration. The solvent for the analytes was methanol (MeOH) and/or acetonitrile (AcCN). The list of analytes and the number of measurements performed for each analyte is summarized in Table 1. In addition to trace standards, some bulk materials ranging in mass from sub-grams to grams were used in the experiments. Multiple measurements were taken under different conditions in order to capture the variabilities related to the method of sample injection, sensor head contamination, aging of the sensing elements, and ambient environment, such as temperature and humidity.

The vapor from the analyte containers was presented to the nozzle of the sensor device for a nominal duration of six seconds. This duration was empirically derived to be long enough to obtain a well-established response (pulse shape) for all the tested analytes and at all concentrations, but short enough to avoid signal saturation and any inconsistency in data statistics caused by the sample introduction process.

Figure 2 illustrates several responses of Fido XT to various analytes. The region of interest, i.e., the portion of the recorded signal that represents the response to be analyzed, is shown within the red vertical lines.

### **3 Signal Processing Approach and Algorithm for Detection and Identification**

The output of Fido XT is a two-channel 20.27 Hz sampled signal stream that represents the change in fluorescence at two locations along the sensing element, which is an AFP-coated

capillary. The raw signals are proportional to the photon count measured at each location. During standard operation of the device, a corresponding quench signal is computed that represents the percentage change in fluorescence intensity relative to an established baseline in the absence of any sample injection. When a material sample is presented to the device with a finite exposure time, the typical response is a “pulse” with material-dependent rise and fall characteristics and potentially a phase lag in the response between the two channels. For the detection of explosives, especially for nitroaromatic compounds, Fido XT’s native detection algorithm is based on the simultaneous observation of a threshold-exceeding quench event and the presence of a phase difference. This simple approach is reasonably accurate for detecting military explosives, such as TNT and RDX. However, detailed examination of the entire response waveforms reveals that pulse pairs for materials beyond traditional military explosives (e.g., urea nitrate, ammonium nitrate) often have different characteristics that do not always successfully trigger detections. Furthermore, certain non-explosive analytes such as musk ketone and di-nitro-o-cresol (DNOC) result in false alarms with the same simple detection approach, although their response waveforms exhibit differences with the military explosives. It is these more subtle waveform characteristics that the algorithmic approach presented in this work exploit.

In the absence of a detailed physical model that predicts the expected response of a sensor to a given set of volatile compounds, machine learning can be used to differentiate between waveforms produced by different analytes. This approach depends critically on the availability of a data corpus representative of the range of analytes that could reasonably

be encountered, including a variety of explosives, explosives-components (oxidizers), and non-explosive materials, as well as potential confusers (i.e., materials that commonly or could be expected to trigger false positive detections or prevent successful detections). The data contained in the corpus should also incorporate sources of variability such as the effects of sensor aging (time-varying performance of the sensor), contamination or degradation of the sensing element by repeated exposure to trace materials, sample presentation dynamics, duration, analyte temperature, and concentration.

A data corpus of 588 analyte samples was collected for this study (Table 1) with sensor signal recordings ranging in duration from about a minute to several minutes. Each recording contains the response produced by a single sample introduction and removal, with a nominal exposure time of six seconds. The region of interest (ROI) in each recording was determined by centering the analysis window around the time of total peak power of the quench signals from the two sensors.

Feature extraction was performed on the raw signals, with vectors derived from the log-magnitude discrete Fourier transform (DFT) of the mean-removed, power normalized, and Hamming-windowed signals over the ROI. In the cases where the ROI window went beyond either ends of the recording, zero-padding was applied. For ROI signals  $s_1(n)$  and  $s_2(n)$ ,  $n=0, \dots, N-1$ , corresponding to the two channels of the recording for a sampling experiment, and their respective  $N$ -point DFTs  $S_1(k)$  and  $S_2(k)$ , the first part of the feature vector  $F$  is comprised of the average of  $\log_{10}|S_1(k)|$  and  $\log_{10}|S_2(k)|$ ,  $k = 0, \dots, N/2-1$ . The second part of feature vector  $F$  is derived from the difference signal, given by  $\log_{10}|S_1(k) -$



$S_2(k)$ ,  $k = 0, \dots, N/2-1$ , resulting in an  $N$ -dimensional vector. This approach for feature extraction yields a compact representation of the characteristics of the average and difference signals.

A DFT length of 512 (25.3 seconds) was found to be adequate to fully contain almost all analyte-response waveforms in the corpus. However, DFT lengths of 256 (12.6 seconds) and 1024 (50.5 seconds) also were examined as potential alternatives in the portion of this work focused on material detection and identification. Partial pulses including only segments up to one second before the quench signal peak within the ROI were also explored as another variation.

The detection of explosive components versus non-explosive materials was implemented using a nearest-neighbor (NN) classification algorithm [5], which also provides a direct means of identification through the labels of the detector library elements for both classes. Given the explosive components class  $E$  and the non-explosive materials class  $N$ , the NN detection decision  $C$  for feature vector  $X$  from an unknown material sample measurement is given by

$$C = \begin{cases} E & \text{if } S \leq T \\ N & \text{if } S > T \end{cases}$$

where

$$S = d_{\min_E} - d_{\min_N}$$

is the differential distance score for the Euclidean distance metric  $D$ , with

$$d_{\min_E} = \min D(\mathbf{X}, \mathbf{X}_{Ej}), j = 1, \dots, M_E,$$

and

$$d_{\min_N} = \min D(\mathbf{X}, \mathbf{X}_{Nj}), j = 1, \dots, M_N$$

where  $X_{Ej}$  denotes the  $j^{\text{th}}$  element in the explosive components class library of  $M_E$  members,  $X_{Nj}$  denotes the  $j^{\text{th}}$  element in the non-explosives class library of  $M_N$  members, and  $T$  is the detection decision threshold for the desired operating point on the ROC curve of detection versus false alarm rates.

Evaluation of the detector was performed using both five-fold and ten-fold cross validation. In five-fold cross validation, training of the algorithm was performed using 80% of available data, followed by testing on the algorithm using the remaining 20%. This was repeated five times (once for each “fold”) so that all of the data was represented in the test set. Similarly, ten-fold cross validation was performed by training on 90% of the available data and testing on the remaining 10%, repeating ten times so that all data was used in the test set. The full corpus of 588 analyte response recordings was used for both partial-pulse and full-pulse cases, and for DFT lengths of 256, 512, and 1024 points. Equal representation of material samples was retained in both the five- and ten-fold cases.

A filter bank on the feature vectors was iteratively trained with a genetic algorithm to optimize (maximize) the area under the ROC curve using a leave-one-out scheme on the training partition. Given all sub-bands of width  $B$  with 50% overlap, one sub-band was dropped in each iteration to obtain the largest improvement in the area under the curve, and iterations ceased when no improvement was possible. Four values of the parameter  $B$  (1/4, 1/8, 1/16, and 1/32 of the full bandwidth) were used for each DFT length. ROC curves on the test partitions were obtained using the pooled differential distance scores for each fold. Performances of both the full-band detectors and the optimized detectors with filter banks composed of the best remaining sub-bands were evaluated.

#### 4 Results and Discussions

The overall results of the detector performance evaluations are given in Table 2. Best detection performance was achieved in ten-fold cross validation trials using a DFT length of 512 points on the full pulse, with 32-point-wide sub-bands used for the optimization step. This yielded an area under the ROC curve of 96.6%, an improvement of about 10% over the non-optimized, full-band detector (area of 88.1%). The equal error rate, or EER (the operating point at which the false positive rate was equal to the false negative or missed detection rate) drops by 52.4% for the full-band detector (i.e., from 20.2% to 9.6%) for the same case (Figure 3). At the end of the optimization step, the number of total DFT frequency bins remaining in the best performing filter banks for the average and difference signals ranged between 112 and 272 for the ten training/testing folds.

Similarly, the five-fold cross validation trials achieved the best area-under-the-curve of 95.4% using the 512-point DFT on the full pulse; this shows an improvement of 8.2% over the non-optimized, full-band detector results (88.2% area-under-the-curve)). The EER in this case dropped by 40.6% (i.e., from 20.2% to 12.0%) for the optimized detector (Figure 4). When the full pulse was used, optimization improved the area-under-the-curve to a greater degree compared to using only the partial pulse (see Table 2). These results indicate that there is significant information in both the rise and decay characteristics of a pulse to help discriminate between explosive components and non-explosive materials. At the end of the optimization step, the number of total DFT frequency bins remaining in the best performing filter banks for the average and difference signals ranged between 120 and 272 for the five training/testing folds.

Even though the detector developed here was optimized for a binary classification task,

examination of the NN-classifier plots reveals that this algorithm also can identify specific materials. Figures 5 and 7 show the confusion plots (detailed breakdown of correct and incorrect identifications) corresponding to the optimized 512-point binary detectors for the ten-fold and five-fold cross-validation cases, respectively. The horizontal axis is the index number for each sample in the data corpus (ranging from 1 to 588). Index ranges outlined in red are explosive materials and components, and those in blue are non-explosive materials. The vertical axis is the index number for the nearest-neighbor match, for a detection decision threshold of  $T = 0$ . This corresponds to an operating point of 93.6% detection at a false alarm rate of 17.6% on the ROC curve for the ten-fold cross-validation trials (Figure 3), while the operating point for the five-fold trials is 91.0% detection at a false alarm rate of 16.3% (Figure 4). A detailed breakdown of the rate of correct and incorrect identifications from these confusion plots are given in Tables 3 and 4, and this data is presented graphically in the summary bar graphs in Figures 6 and 8.

Although the NN classifier was optimized only for classification into explosive and non-explosive materials, there were several analytes for which the NN classifier was able to correctly identify a target with reasonable accuracy. For example, DIMP is perfectly identified in both the ten-fold (Table 3) and five-fold trials (Table 4). DNOC, which an unmodified Fido XT always detects (incorrectly) as a military explosive, is perfectly identified in the ten-fold trials and is misidentified as 2,4-DNT only in 2.1% of the five-fold trials. All twelve  $\text{H}_2\text{O}_2$  samples are correctly identified in the five-fold trials, and only one sample is misidentified as 2,4-DNT in the ten-fold trials. For both DEMP and DPM, only two out of twelve samples are misidentified in both cross-validation trials.

The reference standard device calibration material (a compound of unknown composition

intended to simulate TNT) is identified correctly 83.0% and 89.4% of the time, respectively, for the ten-fold and five-fold cases, and all misidentifications are as TNT. The identification rate for TNT samples is 80.6% for the ten-fold case, with 17.5% misidentified as other explosive materials, and only 1.9% misidentified as non-explosive (musk ketone). For the five-fold case, identification rate for TNT is 71.8%, with a 6.8% rate of misidentification as non-explosives. One out of twelve nitroglycerin samples is misidentified as alcohol in the ten-fold trials, and two samples are misidentified as methanol in the five-fold trials. In both cases one sample is misidentified as 2,4-DNT.

Urea nitrate samples are correctly identified at a rate of 68.7% in the ten-fold trials, but misidentified as non-explosive for 9.0% of the samples. In the five-fold trials, correct identification is 65.7% for the urea nitrate samples, with 11.1% misidentified as non-explosives. Ammonium nitrate samples are misidentified as non-explosives at a rate of 8.2%, while 54.8% are correctly identified in the ten-fold trials. The corresponding rates in the five-fold trials are 11% and 53.4%.

2,4-DNT identification rate is 64.8% with a non-explosive misidentification rate of 12.6% in both the ten-fold and five-fold trials. 2,6-DNT identification rate is 63.3% and 60.0% respectively for the ten-fold and five-fold trials, with a non-explosive misclassification rate of 3.3%.

Musk ketone was always incorrectly identified by the standard (unmodified) Fido XT as a military explosive, but was correctly identified by the NN algorithm at a rate of 38.9% in the ten-fold trials, with the remainder misidentified as TNT. In the five-fold trials, musk ketone is correctly identified at a rate of 66.7%, with the remainder misidentified as either

TNT or reference standard.

## 5 Conclusions

This work develops an algorithm for improving the performance of a mature explosives sensing technology purely via signal processing/ machine-learning, and illustrates its merit through systematic experimental measurements and analysis. This research has examined the output data from Fido XT, an AFP-based explosives sensor, and developed and applied a machine-learning algorithm based on a non-parametric nearest-neighbor binary classification (detection) scheme. Through systematic studies of the response of the sensor to vapors from a large number of explosives components and non-explosive samples, this algorithm has extracted the spectral information content of the waveform and developed a methodology for detection and identification of trace chemicals.

This study demonstrates that the algorithm can enhance the performance of Fido XT by improving both the probability of detection and selectivity. In addition to improved detection, this work has demonstrated that the device can also identify specific materials, with potentially greater identification capability possible through further optimization of the algorithm.

This study concludes that an algorithm-based approach has merits to provide an effective and efficient means for advancing an existing technology, especially to detect and identify new or emerging threat materials. Updating training library with signatures of the new materials, retraining the algorithm and using the same sensing hardware can be performed much rapidly and efficiently than reengineering the device. Finally, pursuing an open set paradigm, further studies with extended data, especially using non-explosive materials with

diverse functional groups (not included in the training sets), are warranted.

### **Acknowledgments**

The work was supported by the U.S. Army under contract W56KGU-15-C-0010. Thanks are due to Geoff Hamshar and Jonathan Buttner for their valuable help in developing communication architecture. The technical assistance of LeRoy Pressley and Gregory Shishmanian in the trace explosives detection laboratory of The MITRE Corporation is thankfully acknowledged.

### **References**

- [1] Ronald L. Woodfin, ed., Trace Chemical Sensing of Explosives, Wiley & Sons, New Jersey, 2007.
- [2] J.I. Steinfeld and J. Wormhoudt, Explosives detection: a challenge for physical chemistry, Annual Review of Physical Chemistry, 49 (1998) 203-32.
- [3] M. Tourné, Developments in explosives characterization and detection, J. Forensic Res. S12 (2013) 1-10.
- [4] D. Ramdasi and R. Mudhawadkar, A review of sensors for explosive detection, International Journal of Scientific & Engineering Research, 4 (2013) 794-798.
- [5] A. Lapointe, Investigation of novel sensor technology for explosive specific detection from a military perspective, December 2009.
- [6] R. O. Duda and P. E. Hart, Pattern Classification and Scene Analysis, John Wiley & Sons, New York, 1973.



- [7] T. Cover and P. Hart, Nearest neighbor pattern classification, IEEE Transactions on Information Theory, 13 (1967) 21-27.
- [8] H. Vincent Poor, An introduction to signal detection and estimation, Springer 2nd Ed., New York, 1988.
- [9] D.W. Hannum and J.E. Parmeter, Survey of commercially available explosives detection technologies and equipment, Sandia National Laboratory Report, September 1998.
- [10] "Existing and potential standoff explosives detection techniques", National Academic Press, 2004.
- [11] "Guidebook on detection technologies and systems for humanitarian demining", March 2006.
- [12] <http://www.flir.com/threatDetection/display/?id=63353>.
- [13] C. Cumming, Explosives Detection Based on Amplifying Fluorescence Polymers, in Trace Chemical Sensing of Explosives ed. R. L. Woodfin John Wiley & Sons, Inc., Hoboken, NJ, USA, 2006.
- [14] R. Ingram and J. Sikes, Trace detection of explosives using an in-line high volume sampler, preconcentrator and Fido explosives detector, Proc. SPIE Conf, 7664 (2010) 7664 15-1 to 7664 15-8.
- [15] M. Fisher and J. Sikes, Minefield edge detection using a novel chemical vapor sensing technique, Proc. SPIE, 5089 (2003) 1078-1087.
- [16] M. Fisher, M. LaGrone, J. Sikes, Implementation of serial amplifying fluorescent polymer arrays for enhanced chemical vapor sensing of landmines, Proc. SPIE, 5089

(2003) 991- 1000.

[17] D.T. McQuade, A. E. Pullen, and T. M. Swager, Conjugated polymer-based chemical sensors, *Chemical Reviews*, 100 (2000) 2537–2574.

[18] J.V. Goodpaster and V.L. McGuffin, Fluorescence quenching as an indirect method for nitrated explosives, *Analytical Chemistry* 73 (2001) 2004-2011.

[19] S.W. Thomas III, J.P. Amara, R.E. Bjork, T.M. Swager, Amplifying fluorescent polymer sensors for the explosives taggant 2,3-dimethyl 1-2,3-dinitrobutane (DMNB), *Chemical Communications*, 36 (2005) 4572-4574.

[20] S.J. Toll and W.C. Trogler, Polymer sensors for nitroaromatic explosive detection, *J. Mater. Chem.* 16 (2006) 2871-2883.

[21] S.W. Thomas, G.D. Joly, and T. M. Swager, Chemical sensors based on amplifying fluorescent conjugated polymers, *Chemical Reviews* 107 (2007) 1339–1386.

[22] R. Anandakathir, A. Kumar, and J. Kumar, Novel fluorescent polymer for trace explosive detection, *Proc. IEEE Conference on Technologies for Homeland Security*, pp. 319-322, 2009.

[23] G.B. Demirel, B. Daglar, and M. Bayindir, Extremely fast and highly selective detection of nitroaromatic explosive vapors using fluorescent polymer thin films, *Chemical Communications*, 49 (2013) 6140-6142.

[24] F. Chu, G. Tsiminis, N.A. Spooner, and T.M. Monro, Explosives detection by fluorescence quenching of conjugated polymers in suspended core optical fibers, *Sensors and Actuators B: Chemical* 199 (2014) 22-26.

**Burhan Necioglu**

Burhan F. Necioglu is with The MITRE Corporation. He received his Ph.D. in Electrical Engineering from the Georgia Institute of Technology in 1999, his M.S. in Electrical Engineering from Boston University in 1992, and his B.S. in Electrical Engineering from the Middle East Technical University in 1989. His research interests include machine learning and its applications to multi-dimensional and multi-modal signals.

**Wansheng Su**

Wansheng Su received his Ph.D. in Electrical Engineering from Virginia Polytechnic Institute and State University in 1993. His research interests are non-destructive materials characterization and molecular spectroscopy (energy dispersive, ion mobility, infrared reflection, and Raman).

**Jefferson Rhodes**

Jefferson M. Rhodes received a B.S. degree in Computer Engineering and a M.E. degree in Electrical Engineering from the University of Virginia, in 2002 and 2004 respectively. Since then, he has been with The MITRE Corporation where he is currently a member of the Electronics Systems Development division. He has a background in FPGA and embedded software development ranging in applications for software-defined radios, radar, signal processing, error correction coding, network intrusion detection, and cryptography.

**Sarah O'Donnell****Mark Taczak**

Mark Taczak is a Principal Multi-Discipline Systems Engineer in MITRE's Emerging Technologies department. He received his B.S. in Materials Science and Engineering from Virginia Tech, and an M.E. in Systems Engineering from the University of Virginia. His professional and research interests include nanotechnology, MEMS, robotics, biotechnology, and remote sensing.

**Samar K. Guharay**

As a principal scientist at the MITRE Corporation Dr. Samar K. Guharay (Ph.D. Physics, 1980, University of Calcutta, India) has been leading several R&D activities in the area of trace explosive and chemical detection, algorithms, and systems engineering. He is an Adjunct Professor of the Chemistry Department, Washington State University and Industrial Advisory Board member, Electrical and Computer Engineering Department, Old Dominion University. As an Affiliate Professor of George Mason University he offered a graduate course on Nanocharacterization. From 1984 to 2000 his research at the University of Maryland College Park focused on sub-mm wave spectroscopy, negative ion beam transport and sub-micrometer focused ion beams.

**FIGURE CAPTIONS:**

Figure 1: Schematic of the experimental arrangement. Samples are drawn from ambient air into the AFP sensing element. The system control and signal processing unit controls the sensor functionality and determines if targeted materials, here trace explosives, are detected.

Figure 2: Measured response for different materials. Here raw data are presented. The vertical axis corresponds to photon counts (in arbitrary units) and the horizontal axis represents time in seconds. The two traces (in green and blue color) correspond to response from the two sensing zones, i.e., front and back. The region of interest (ROI) is within the two vertical red lines, which corresponds to a window length of 512 sample points in this example.

Figure 3: Combined ROC curve for *ten-fold* cross-validation experiments. Feature extraction on full pulse using 512-pt DFT with 32-pt sub-bands for optimization on each training fold.

Figure 4: Combined ROC curve for *five-fold* cross-validation experiments. Feature extraction on full pulse using 512-pt DFT with 16-pt sub-bands for optimization on each training fold.

Figure 5: Combined confusion plot for nearest-neighbor classification experiments using *ten-fold* cross-validation, with feature extraction on full pulse using 512-pt DFT and sub-bands optimized for detection. Corresponding operating point is 93.6% detection at a false alarm rate of 17.6%. Red color denotes the explosives components class, and blue denotes the non-explosive

confusers. Green circles are misclassifications within the correct detection class; magenta circles represent misclassifications corresponding to missed detections and false alarms.

Figure 6: Correct identification rates for nearest-neighbor classification experiments using *ten-fold* cross-validation, with feature extraction on full pulse using 512-pt DFT and sub-bands optimized for detection. Corresponding operating point is 93.6% detection at a false alarm rate of 17.6%. Red color denotes the explosives components class, and blue denotes the non-explosive confusers. Average correct identification rate is 73.0%.

Figure 7: Combined confusion plot for nearest-neighbor classification experiments using *five-fold* cross-validation, with feature extraction on full pulse using 512-pt DFT and sub-bands optimized for detection. Corresponding operating point is 91.0% detection at a false alarm rate of 16.3%. Red color denotes the explosives components class, and blue denotes the non-explosive confusers. Green circles are misclassifications within the correct detection class; magenta circles represent misclassifications corresponding to missed detections and false alarms.

Figure 8: Correct identification rates for nearest-neighbor classification experiments using *five-fold* cross-validation, with feature extraction on full pulse using 512-pt DFT and sub-bands optimized for detection. Corresponding operating point is 91.0% detection at a false alarm rate of 16.3%. Red color denotes the explosives components class, and blue denotes the non-explosive confusers. Average correct identification rate is 71.4%.

**TABLE CAPTIONS:**

Table 1: Materials used in the study

Table 2: Detection performance comparison on the data corpus of Table 1

Table 3: Confusion matrix (in %) for nearest-neighbor classification experiments using *ten-fold* cross-validation, with feature extraction on full pulse using 512-pt DFT and sub-bands optimized for detection. Corresponding operating point is 93.6% detection at a false alarm rate of 17.6%.

Table 4: Confusion matrix (in %) for nearest-neighbor classification experiments using *five-fold* cross-validation, with feature extraction on full pulse using 512-pt DFT and sub-bands optimized for detection. Corresponding operating point is 91% detection at a false alarm rate of 16.3%.

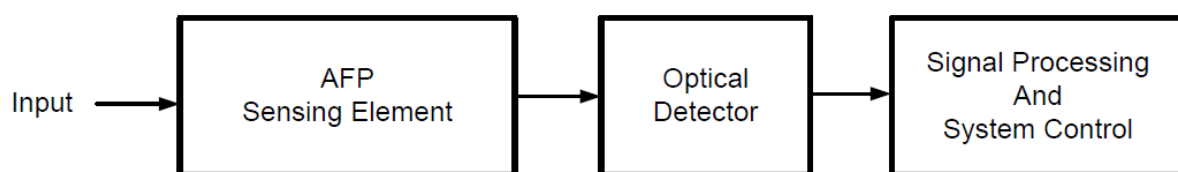


Figure 1: Schematic of the experimental arrangement. Samples are drawn from ambient air into the AFP sensing element. The system control and signal processing unit controls the sensor functionality and determines if targeted materials, here trace explosives, are detected.



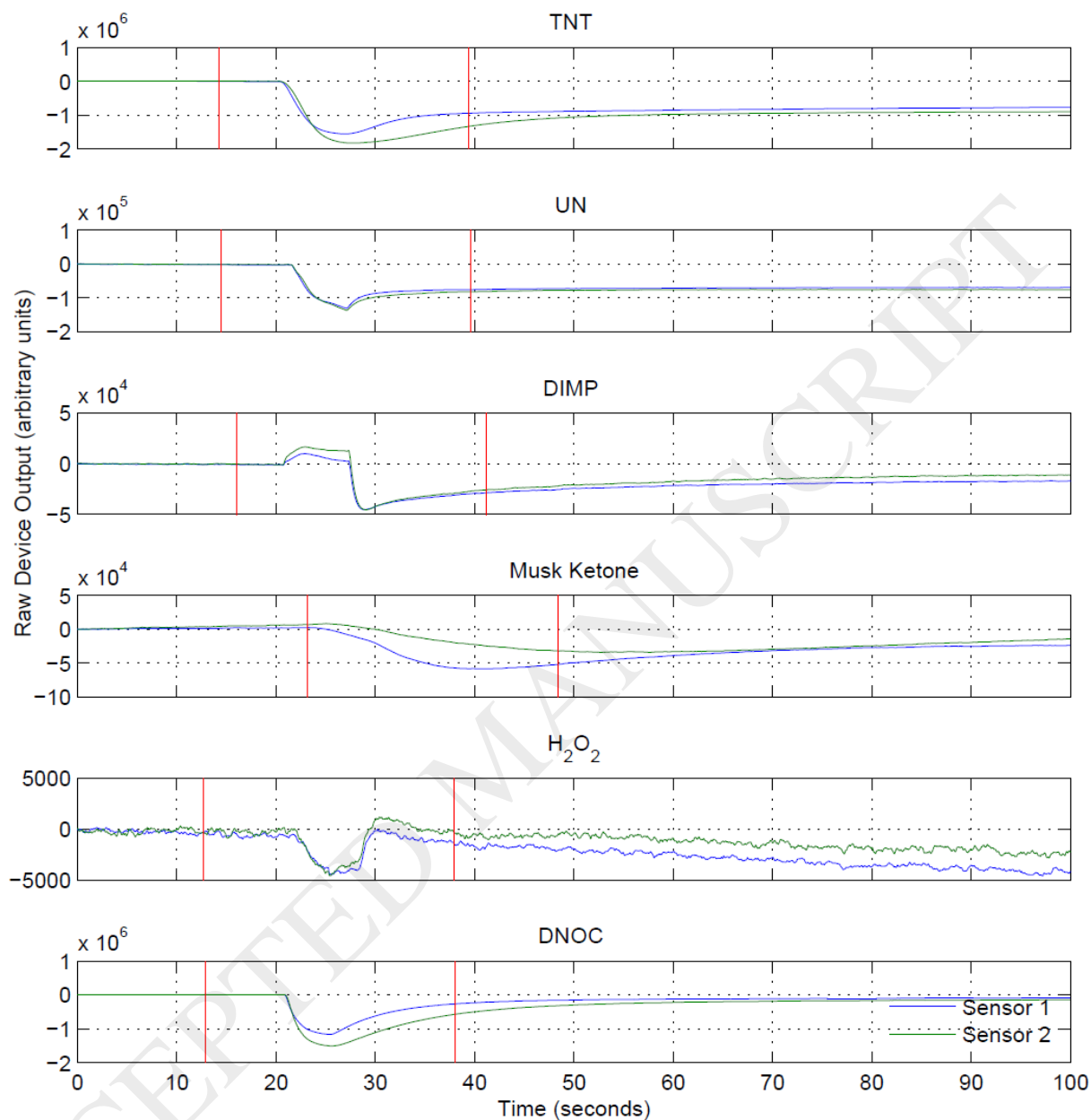


Figure 2: Measured response for different materials. Here raw data are presented. The vertical axis corresponds to photon counts (in arbitrary units) and the horizontal axis represents time in seconds. The two traces (in green and blue color) correspond to response from the two sensing zones, i.e., front and back. The region of interest (ROI) is within the two vertical red lines, which corresponds to a window length of 512 sample points in this example.

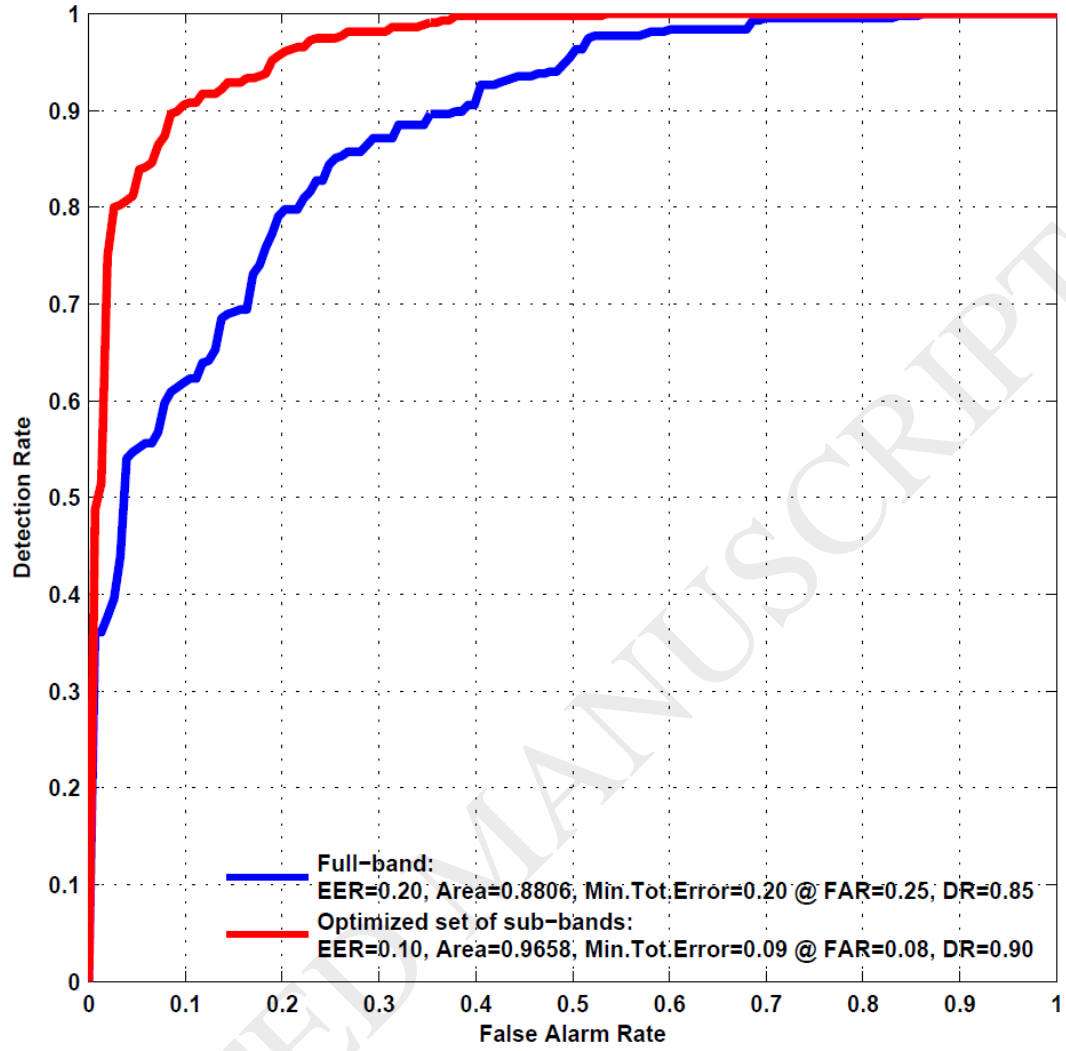


Figure 3: Combined ROC Curve for *ten-fold* cross-validation experiments. Feature extraction on full pulse using 512-pt DFT with 32-pt sub-bands for optimization on each training fold.

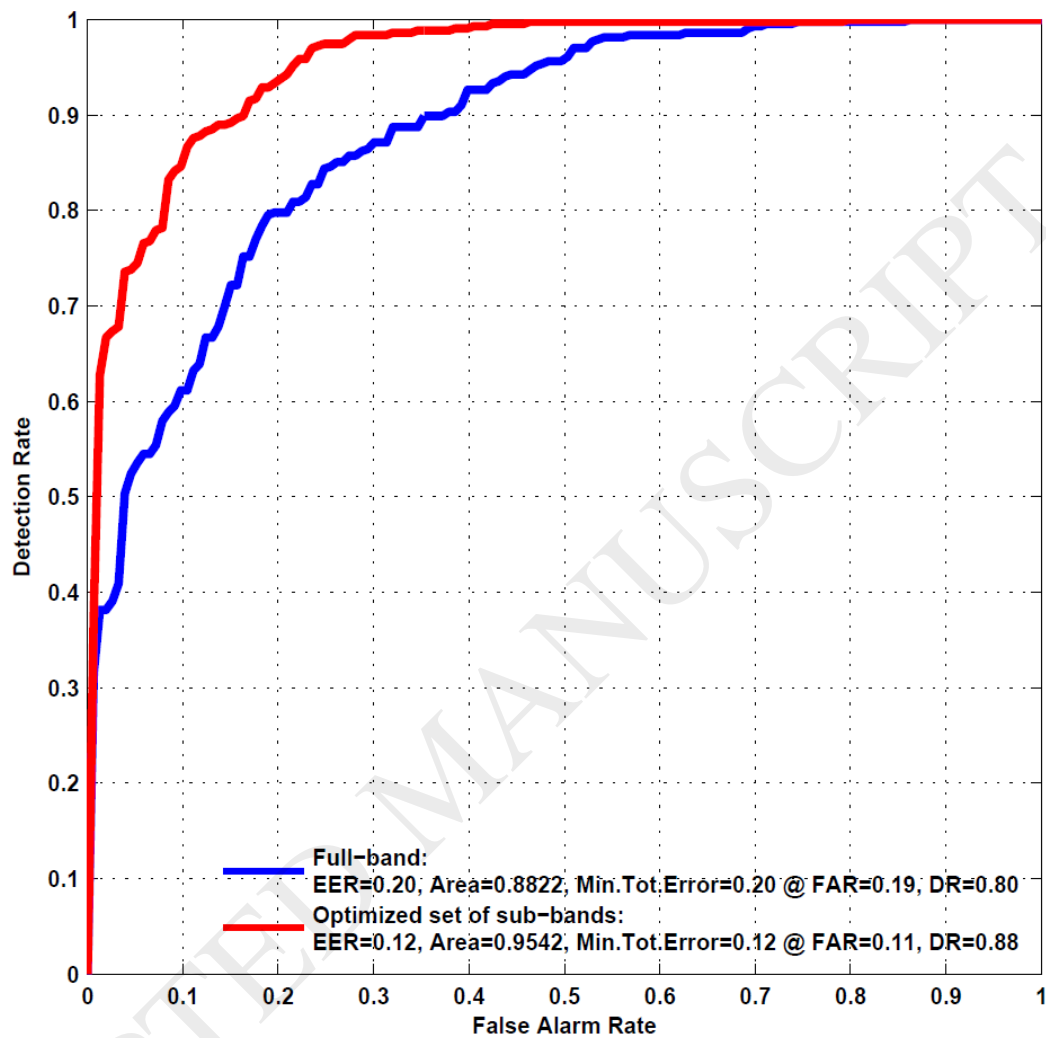


Figure 4: Combined ROC Curve for *five-fold* cross-validation experiments. Feature extraction on full pulse using 512-pt DFT with 16-pt sub-bands for optimization on each training fold.

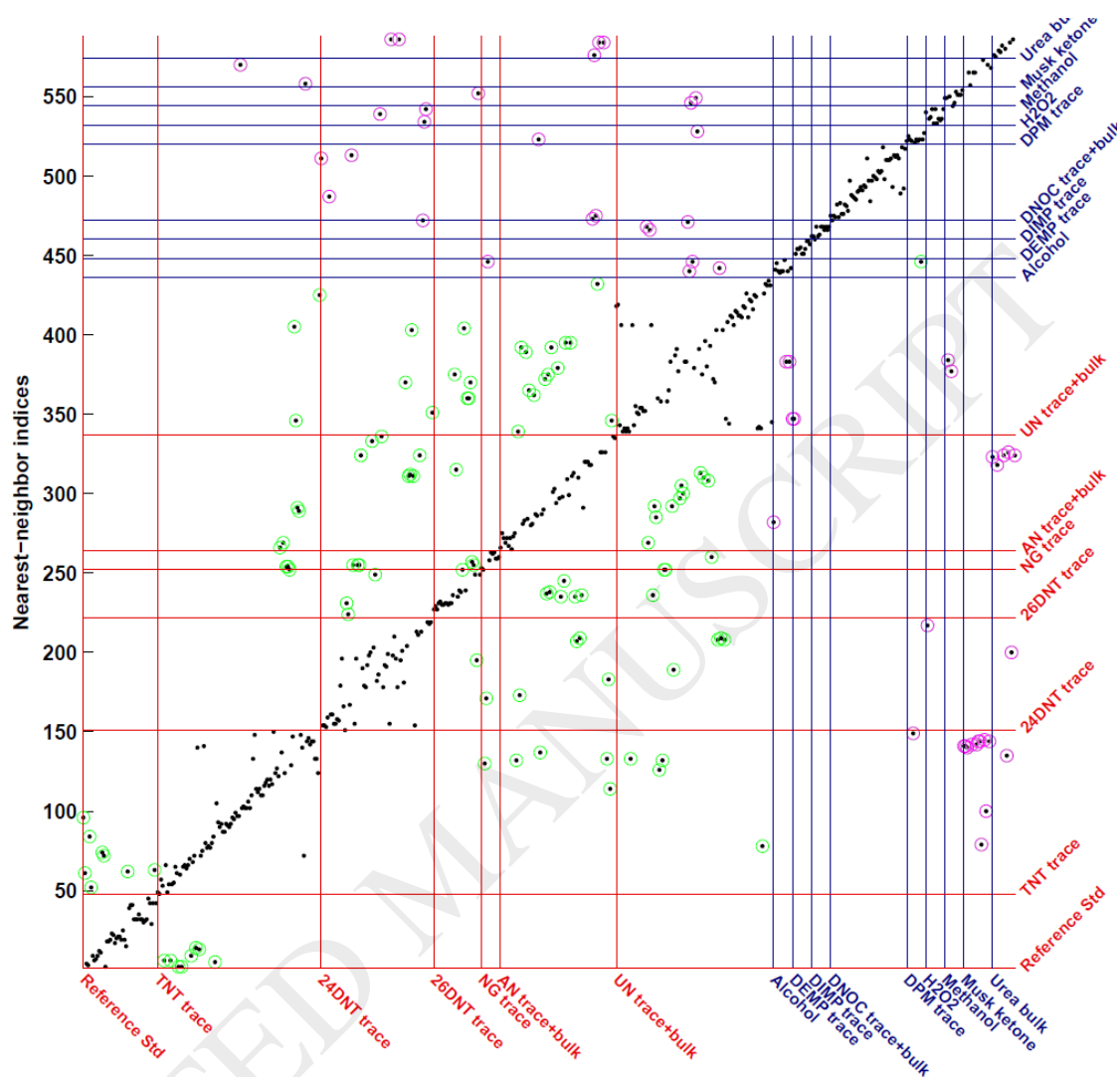


Figure 5: Combined confusion plot for nearest-neighbor classification experiments using *ten-fold* cross-validation, with feature extraction on full pulse using 512-pt DFT and sub-bands optimized for detection. Corresponding operating point is 93.6% detection at a false alarm rate of 17.6%. Red color denotes the explosives components class, and blue denotes the non-explosive confusers. Green circles are misclassifications within the correct detection class, magenta circles represent misclassifications corresponding to missed detections and false alarms.

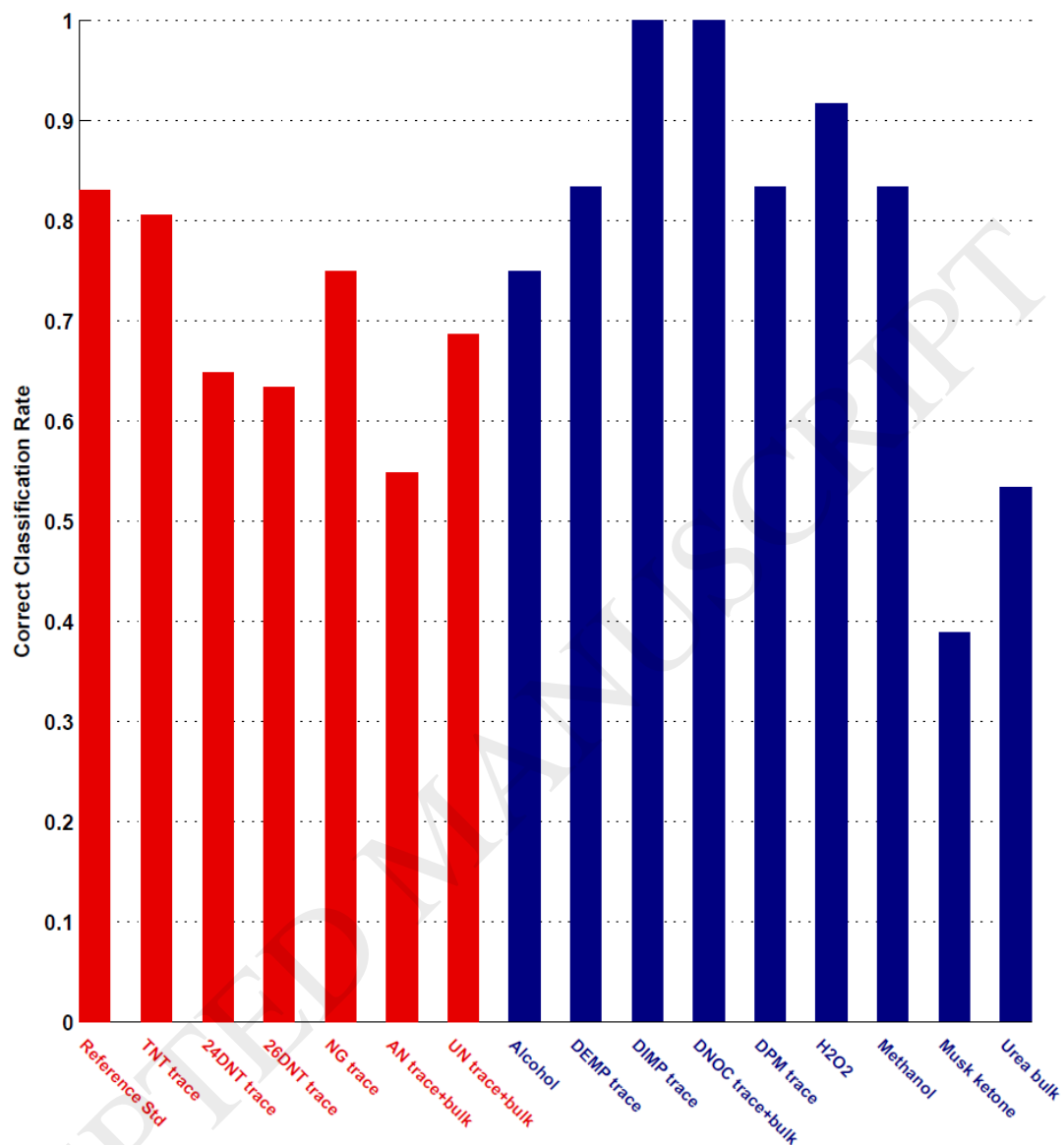


Figure 6: Correct identification rates for nearest-neighbor classification experiments using *ten-fold* cross-validation, with feature extraction on full pulse using 512-pt DFT and sub-bands optimized for detection. Corresponding operating point is 93.6% detection at a false alarm rate of 17.6%. Red color denotes the explosives components class, and blue denotes the non-explosive confusers. Average correct identification rate is 73.0%.

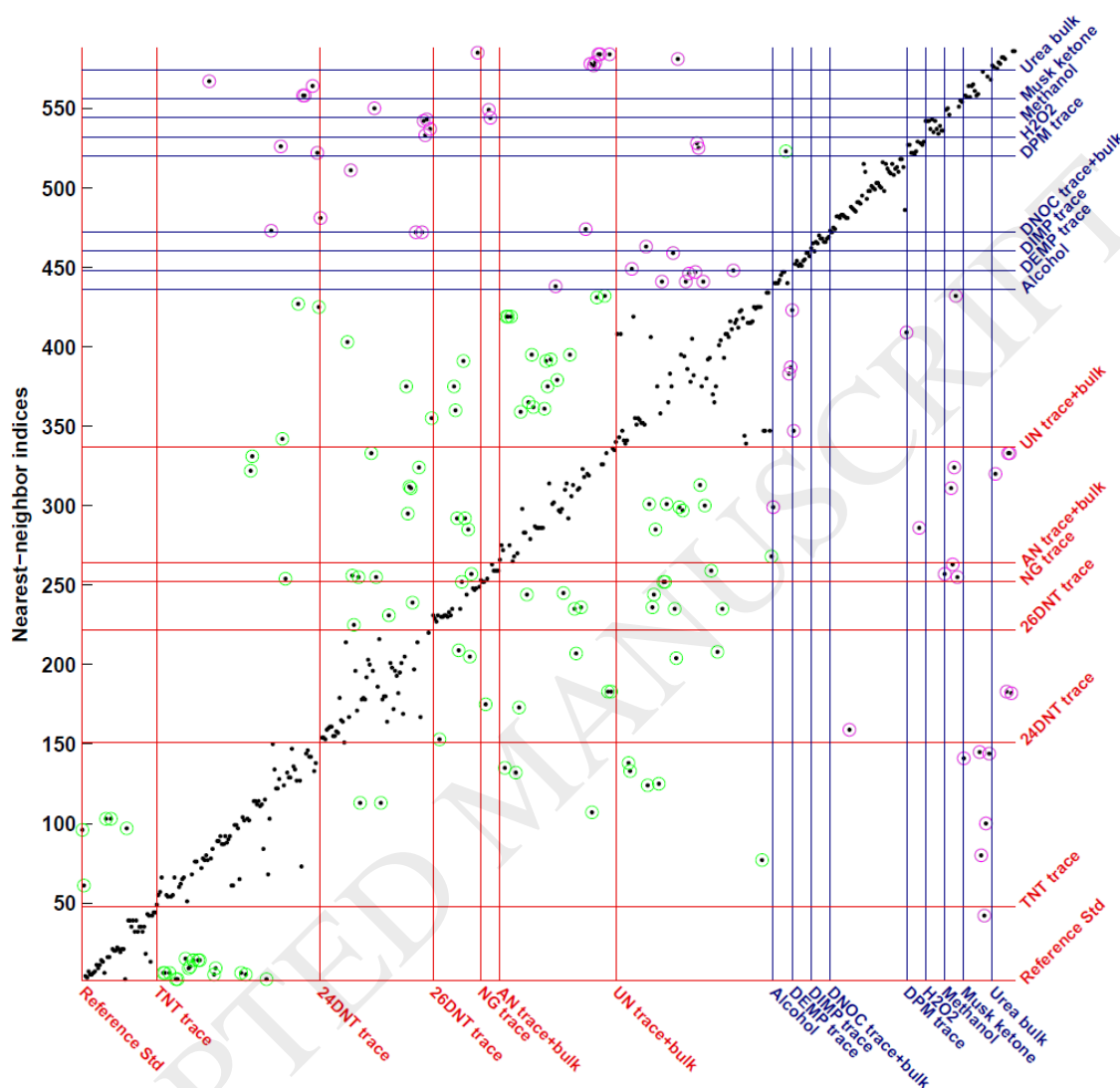


Figure 7: Combined confusion plot for nearest-neighbor classification experiments using *five-fold* cross-validation, with feature extraction on full pulse using 512-pt DFT and sub-bands optimized for detection. Corresponding operating point is 91.0% detection at a false alarm rate of 16.3%. Red color denotes the explosives components class, and blue denotes the non-explosive confusers. Green circles are misclassifications within the correct detection class, magenta circles represent misclassifications corresponding to missed detections and false alarms.

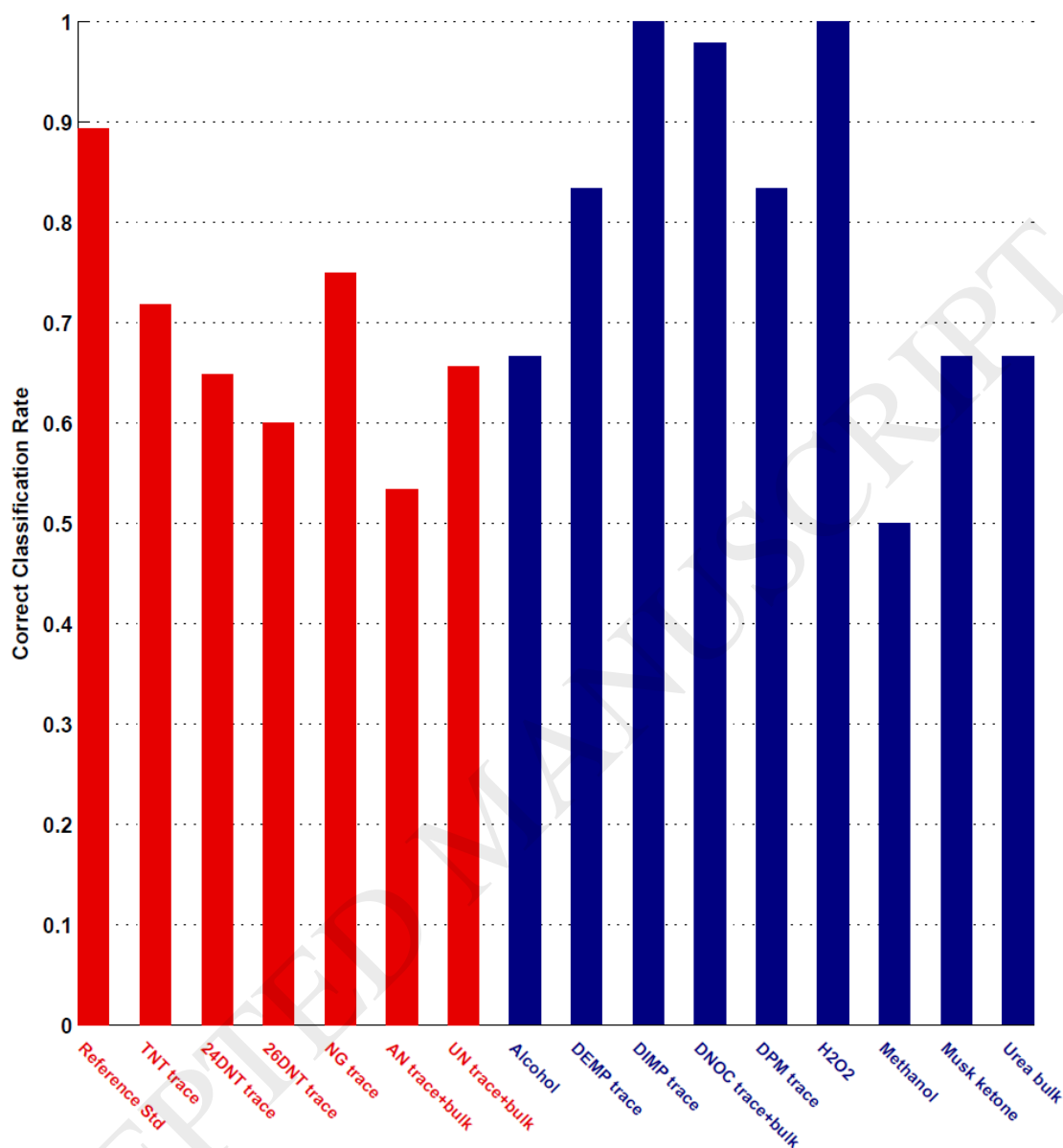


Figure 8: Correct identification rates for nearest-neighbor classification experiments using *five-fold* cross-validation, with feature extraction on full pulse using 512-pt DFT and sub-bands optimized for detection. Corresponding operating point is 91.0% detection at a false alarm rate of 16.3%. Red color denotes the explosives components class, and blue denotes the non-explosive confusers. Average correct identification rate is 71.4%.

Table 1

<b>Explosives Components</b>	<b>Samples</b>
Reference Standard (REF) (device calibration material similar to TNT)	47
Trinitrotoluene (TNT) trace (1 mg/ml, 0.1 mg/ml, 0.01 mg/ml)	103
2,4-Dinitrotoluene (2,4-DNT) trace (1 mg/ml, 0.1 mg/ml)	71
2,6-Dinitrotoluene (2,6-DNT) trace (1 mg/ml, 0.1 mg/ml)	30
Nitroglycerin (NG) trace (1 mg/ml)	12
Ammonium nitrate (AN) trace (1 mg/ml, 0.1 mg/ml, 0.01 mg/ml) & bulk (oxidizer)	73
Urea nitrate (UN) trace (1 mg/ml, 0.1 mg/ml, 0.01 mg/ml) & bulk	99
<b>Total</b>	<b>435</b>
<b>Non-explosives</b>	<b>Samples</b>
Alcohol	12
Diethyl methylphosphonate (DEMP) trace (1 mg/ml)	12
Diisopropyl methylphosphonate (DIMP) trace (1 mg/ml)	12
Dinitro-o-cresol (DNOC) trace (1 mg/ml) & bulk	48
Dipropylene glycol monomethyl ether (DPM) trace (1 mg/ml)	12
H <sub>2</sub> O <sub>2</sub>	12
Methanol (MeOH)	12
Musk ketone (MK) bulk	18
Urea bulk	15
<b>Total</b>	<b>153</b>



Table 2

Cross Valida- tion	Analysis Pulse	DFT Size	Opti- mization Sub-band Width	Area Under ROC Curve (%)		Equal Error Rate (%)	
				Full Band	Best sub- bands	Full Band	Best sub- bands
5-fold	Partial	256	4	86.6	89.0	22.2	19.5
5-fold	Partial	512	16	82.2	85.1	27.7	24.7
5-fold	Partial	1024	128	85.0	88.2	23.8	20.9
5-fold	Full	256	16	88.2	94.7	19.1	10.9
5-fold	Full	512	16	88.2	95.4	20.2	12.0
5-fold	Full	1024	32	87.3	93.5	20.7	13.4
10-fold	Partial	256	16	86.5	88.7	23.3	21.1
10-fold	Partial	512	8	80.9	84.4	29.2	24.1
10-fold	Partial	1024	128	84.0	87.8	25.1	20.8
10-fold	Full	256	16	86.9	95.8	21.2	10.3
10-fold	Full	512	32	88.1	96.6	20.2	9.6
10-fold	Full	1024	64	87.0	94.6	20.5	13.1

Table no.3

Identified as Material	2,4-DNT	2,6-DNT	AN	Alcohol	DEMP	DIMP	DNOC	DPM	H <sub>2</sub> O <sub>2</sub>	MeOH	MK	NG	REF	TNT	UN	Urea
2,4-DNT	64.8	4.2	9.9	0.0	0.0	0.0	5.6	0.0	4.2	0.0	0.0	4.2	0.0	0.0	4.2	2.8
2,6-DNT	3.3	63.3	<b>3.3</b>	0.0	0.0	0.0	0.0	0.0	0.0	3.3	0.0	10.0	0.0	0.0	16.7	0.0
AN	5.5	8.2	<b>54.8</b>	0.0	0.0	0.0	2.7	1.4	0.0	0.0	0.0	0.0	0.0	5.5	17.8	4.1
Alcohol	0.0	0.0	8.3	<b>75.0</b>	0.0	0.0	0.0	0.0	0.0	0.0	0.0	0.0	0.0	0.0	16.7	0.0
DEMP	0.0	0.0	0.0	0.0	<b>83.3</b>	0.0	0.0	0.0	0.0	0.0	0.0	0.0	0.0	0.0	16.7	0.0
DIMP	0.0	0.0	0.0	0.0	0.0	<b>100.0</b>	0.0	0.0	0.0	0.0	0.0	0.0	0.0	0.0	0.0	0.0
DNOC	0.0	0.0	0.0	0.0	0.0	0.0	<b>100.0</b>	0.0	0.0	0.0	0.0	0.0	0.0	0.0	0.0	0.0
DPM	0.0	0.0	0.0	8.3	0.0	0.0	0.0	<b>83.3</b>	0.0	0.0	0.0	0.0	0.0	8.3	0.0	0.0
H <sub>2</sub> O <sub>2</sub>	8.3	0.0	0.0	0.0	0.0	0.0	0.0	0.0	<b>91.7</b>	0.0	0.0	0.0	0.0	0.0	0.0	0.0
MeOH	0.0	0.0	0.0	0.0	0.0	0.0	0.0	0.0	0.0	<b>83.3</b>	0.0	0.0	0.0	0.0	16.7	0.0
MK	0.0	0.0	0.0	0.0	0.0	0.0	0.0	0.0	0.0	0.0	<b>38.9</b>	0.0	0.0	61.1	0.0	0.0
NG	8.3	0.0	0.0	8.3	0.0	0.0	0.0	0.0	0.0	0.0	0.0	<b>75.0</b>	0.0	8.3	0.0	0.0
REF	0.0	0.0	0.0	0.0	0.0	0.0	0.0	0.0	0.0	0.0	0.0	0.0	<b>83.0</b>	17.0	0.0	0.0
TNT	0.0	0.0	3.9	0.0	0.0	0.0	0.0	0.0	0.0	0.0	1.9	2.9	7.8	<b>80.6</b>	2.9	0.0
UN	4.0	1.0	10.1	3.0	0.0	3.0	0.0	1.0	0.0	2.0	0.0	3.0	0.0	4.0	<b>68.7</b>	0.0
Urea	6.7	0.0	33.3	0.0	0.0	0.0	0.0	0.0	0.0	0.0	0.0	0.0	0.0	6.7	0.0	<b>53.3</b>

